

The Anatomy of $K^+ \rightarrow \pi^+ \nu \bar{\nu}$ Distributions

Martin Gorbahn^{*a}, Ulserik Moldanazarova^{†a,b}, Kai Henryk Sieja^{‡c},
Emmanuel Stamou^{§c}, Mustafa Tabet^{¶c}

^a*Department of Mathematical Sciences, University of Liverpool, Liverpool L69 3BX, UK*

^b*Faculty of Physics and Technology, Karaganda Buketov University, 100028 Karaganda, Kazakhstan*

^c*Fakultät für Physik, TU Dortmund, D-44221 Dortmund, Germany*

December 10, 2023

Abstract

The excellent experimental prospects to measure the invisible mass spectrum of the $K^+ \rightarrow \pi^+ \nu \bar{\nu}$ decay opens a new path to test generalised quark–neutrino interactions with flavour changing $s \rightarrow d$ transitions and as such to novel probes of Physics beyond the Standard Model. Such signals can be a consequence of new lepton-number violating or lepton-number conserving interactions, with their interpretations depending on the Majorana versus Dirac nature of the neutrinos. Furthermore, the possible existence of new massive sterile neutrinos can be tested via their distinctive imprints in the invariant mass spectrum. Within the model-independent framework of the weak effective theory at dimension-six, we study the New Physics effects of Majorana and Dirac neutrinos on the differential distribution of $K^+ \rightarrow \pi^+ \nu \bar{\nu}$ allowing for lepton-number violating interactions and potential new sterile neutrinos. We determine the current and expected future sensitivity on the corresponding Wilson coefficients using the distribution measured by the NA62 collaboration and accounting for expected improvements based on the HIKE experiment. We present single-operator fits and also determine correlations among different type of operators. Even though we focus on $s \rightarrow d \nu \bar{\nu}$ transitions, the operator bases for Majorana and Dirac and the classification of lepton-number-violating/conserving interactions is applicable also for the study of $b \rightarrow s/d \nu \bar{\nu}$ and $c \rightarrow u \nu \bar{\nu}$ transitions relevant in current phenomenology.

^{*}mgorbahn@liverpool.ac.uk

[†]psumolda@liverpool.ac.uk

[‡]kai.sieja@tu-dortmund.de

[§]emmanuel.stamou@tu-dortmund.de

[¶]mustafa.tabet@tu-dortmund.de

Contents

1	Introduction	1
2	Weak effective theories for $K \rightarrow \pi \nu \bar{\nu}$	2
2.1	Majorana- ν EFT with lepton-number violation	4
2.2	Dirac- ν EFT with lepton-number conservation	5
3	Rates and distributions for $K^+ \rightarrow \pi^+ \nu \bar{\nu}$ at NA62	6
3.1	Decay rates	6
3.2	Statistical treatment for EFT fit	9
4	New Physics sensitivities	10
4.1	Single-operator fits	11
4.2	Multi-operator correlations	14
5	Discussion and conclusions	14
A	Decay rates	18
	References	20

1 Introduction

The branching ratio of the rare $K^+ \rightarrow \pi^+ \nu \bar{\nu}$ decay is currently being measured at $\mathcal{O}(35\%)$ accuracy at the NA62 experiment [1, 2], while improved upper limits for the corresponding neutral decay mode, $K_L \rightarrow \pi^0 \nu \bar{\nu}$, are provided from the KOTO experiment [3, 4]. Each event of the charged decay mode has a so-called missing neutrino mass squared, which leads to a decay spectrum that can be measured with increased experimental statistics. The existing measurements already play an important role in current phenomenology. They are sensitive to modifications of the Standard Model (SM) that are generated via effective operators at $\mathcal{O}(100 \text{ TeV})$ and also constrain feebly interacting particles that can provide new final states contributing to the invisible mass spectrum [5, 6].

This exceptional sensitivity to New Physics (NP) is due to the high suppression of these decay rates in the SM and the precision reached in their theory predictions. Both rare $K \rightarrow \pi \nu \bar{\nu}$ decay modes are flavour-changing neutral-current (FCNC) processes, and as such loop-induced in the SM and additionally suppressed by products of off-diagonal Cabibbo–Kobayashi–Maskawa Matrix (CKM) elements. The fact that the neutrinos are only interacting with the weak sector of the SM results in a hard Glashow–Iliopoulos–Maiani (GIM) mechanism [7], which highly suppresses light-quark contributions. This generates a severe CKM suppression in the SM and facilitates a precise theory prediction, where, to a very good approximation, only a single local charged-current operator contributes below the charm scale. The evaluation of the operator matrix element and its Wilson coefficient through an ongoing theoretical effort has lead to a theory uncertainty of only 3% and 1% for the charged and neutral decay modes, respectively [8–13]. This uncertainty includes the contribution of higher-dimensional operators and light-quark contributions, which have been estimated in chiral perturbation theory [14] and can be evaluated on the lattice [15, 16]. The overall uncertainty in the current SM prediction for the charged decay mode [17] is still dominated by the CKM input parameters, yet current input values [18] result in an overall theory uncertainty of $\simeq 6\%$. This has to be compared with the expected uncertainty of 15% and 5% for the branching-ratio measurement at the end of NA62 and after the first

phase of the proposed HIKE experiment [19], respectively. These improved measurements, together with the ones for the K_L mode [20], will result in even tighter probes of potential NP scenarios with flavour violation in the $s - d$ sector.

The present work is motivated by the fact that a more detailed measurement of the missing-mass spectrum will become available at the end of the NA62 experiment and during the run of HIKE. In anticipation of this data, we will consider scenarios with heavy NP, including the possibility of additional massive sterile neutrinos, that can impact the missing-mass spectrum of $K^+ \rightarrow \pi^+ \nu \bar{\nu}$. We discuss their effect in a mostly model-independent manner by considering all the relevant weak effective theory operators up to dimension six for both Majorana and Dirac neutrinos. Here, non-zero contributions of (pseudo-)scalar and tensor operators can distinctively modify the invariant mass spectrum from the SM-like spectrum generated by vector and axial-vector operators. These generalised neutrino interactions have recently received considerable attention in the context of neutrino oscillations [21–24] and correlations to charged current decays have for example been studied in Ref. [25] in the context of SMEFT. In this work, we will study their impact on the FCNC golden Kaon decay. The impact of sterile neutrinos on (axial-)vector type operators has been studied in Ref. [26]. Working with the two, physically distinct scenarios of Dirac and Majorana neutrinos allows us to incorporate mass effects of sterile neutrinos for all operators, which would not be possible in a basis where neutrinos are represented as Weyl fields [27]. This distinction has the benefit of providing a transparent interpretation of a possible NP signal in terms of lepton-number conserving or lepton-number violating NP interactions. Dirac and Majorana weak effective theories originate from different UV theories. E.g., in the Standard Model Effective Field Theory (SMEFT) only three Majorana neutrinos are present in the weak effective theory. Constraints on scalar-type SMEFT operators on the $K^+ \rightarrow \pi^+ \nu \bar{\nu}$ distributions were partially studied in Ref. [28], but an analysis that incorporates the experimental cuts and backgrounds is hitherto missing. To incorporate the full experimental information we derive the differential decay rate as a function of the pion momentum and the invariant neutrino mass in the lab frame of NA62 for Majorana and Dirac neutrinos including mass effects and allowing for flavour-violation in the neutrino sector. We then perform a full statistical analysis of the sensitivity to probe the different NP Wilson coefficients accounting for the single-event sensitivity and available background information at the current and future-planned experimental setup.

The paper is organised as follows. In Section 2 we classify the weak effective theory relevant for $q \rightarrow q' \nu \bar{\nu}$ FCNCs and count the independent Wilson coefficients that contribute to flavour-changing quark into neutrino decays. In the following Section 3 we provide the relevant decay rates for zero neutrino masses, and explain our statistical treatment including the treatment of theoretical uncertainties. In the next Section 4 we provide the current and expected future sensitivities for the cases in which a single operator contributes (single-operator fits) as well as the correlated constraints on pairs of different operators. After the conclusion we also provide in Appendix A further formulae for the double differential distributions $d^2\text{Br}/dq^2 dk^2$.

2 Weak effective theories for $K \rightarrow \pi \nu \bar{\nu}$

The focus of this work is to study the possible impact of heavy New Physics (NP) scenarios in the distributions of $K^+ \rightarrow \pi^+ \nu \bar{\nu}$. The goal is to also include the possibility that the existence of additional heavy neutrinos could provide further final states with missing energy. To this end, it is useful and necessary to distinguish the conceptually different cases of having Majorana-type versus Dirac-type neutrino masses for the three light neutrinos or the possible extra sterile neutrinos. Both Majorana and Dirac operator basis have a direct correspondence in terms of the basis written using chiral (or

equivalently two-component Weyl) fermion fields [27]. However, unless the dimension-four mass terms are specified, the chiral basis with more than three neutrino fields leaves the question of neutrino masses unspecified: The additional right-handed neutrinos can combine with the left-handed ones to give Dirac masses without the need for lepton-number-violating mass terms. Alternatively, the observed neutrinos are Majorana particles in which case their masses originate from Majorana mass terms and the extra, sterile neutrinos have their own independent mass.

We will thus separately discuss two cases:

- (i) Three or more Majorana neutrinos with dimension-six interactions with $s - d$ FCNC interactions that can include lepton-number violation.
- (ii) Dirac neutrinos with dimension-six interactions with $s - d$ FCNC interactions that conserve lepton-number.

Each of these cases will have a distinct low-energy effective theory. We thus decompose the effective Lagrangian relevant for quark-FCNC transitions with neutrinos, i.e., $d_i \rightarrow d_j \nu \nu$ or $u_i \rightarrow u_j \nu \nu$, at the dimension-six level as

$$\mathcal{L}_{q \rightarrow q' \nu \nu}^{\nu \text{LEFT}} \Big|_{\nu\text{-type}} = \mathcal{L}_{\text{QCD}}^{(4)} + \mathcal{L}_{\nu}^{(4)} \Big|_{\nu\text{-type}} + \mathcal{L}_{q \rightarrow q' \nu \nu}^{(6), \text{SM}} + \mathcal{L}_{q \rightarrow q' \nu \nu}^{(6)} \Big|_{\nu\text{-type}}, \quad (1)$$

where the superscript “(n)” indicates the mass-dimension of the operators and ν -type labels the case of Majorana or Dirac neutrinos. Apart from the usual dimension-four QCD Lagrangian involving quarks and gluons, the kinetic and mass term of the neutrinos reads

$$\mathcal{L}_{\nu}^{(4)} \Big|_{\text{Majorana}} = \frac{1}{2} \sum_a \bar{\nu}_{Ma} (i \not{\partial} - M_a) \nu_{Ma}, \quad \mathcal{L}_{\nu}^{(4)} \Big|_{\text{Dirac}} = \sum_a \bar{\nu}_{Da} (i \not{\partial} - M_a) \nu_{Da}, \quad (2)$$

where $a \geq 3$ runs over the different neutrino flavours, and ν_{Ma} and ν_{Da} denote four-component Majorana and Dirac fields, respectively. Eq. (2) is already written in terms of mass-eigenstates for the neutrinos fields. Throughout this work we work in the mass-eigenstate basis for the neutrinos. This choice of basis implicitly also fixes the basis for the definition of the dimension-six Wilson coefficients.

In the present work we focus on $K \rightarrow \pi \nu \nu$. In this case the SM induces a single dimension-six operator below the charm mass [17, 29]. For the $s \rightarrow d$ transition the SM contribution can be written both in terms of Majorana or Dirac fields

$$\begin{aligned} \mathcal{L}_{s \rightarrow d \nu \nu}^{(6), \text{SM}} &= \sum_{a, b = \{1, 2, 3\}} \left\{ \begin{array}{l} C_{ab21}^{A, L, \text{SM}} O_{ab21}^{A, L} \\ C_{ab21}^{V, LL, \text{SM}} O_{ab21}^{V, LL} \end{array} \right\} + \text{h.c.} \\ &= -\frac{4G_F}{\sqrt{2}} \frac{\alpha}{2\pi s_w^2} \sum_{\substack{\ell = \{e, \mu, \tau\} \\ a, b = \{1, 2, 3\}}} U_{\ell a}^* U_{\ell b} \left(\lambda_c X^\ell + \lambda_t X_t \right) \times \left\{ \begin{array}{l} -O_{ab21}^{A, L} \\ O_{ab21}^{V, LL} \end{array} \right\} + \text{h.c.}, \end{aligned} \quad (3)$$

where G_F denotes the Fermi constant, α is the fine-structure constant, and s_w is the sine of the weak-mixing angle. The elements of the quark-mixing matrix are comprised in the parameters $\lambda_i = V_{is}^* V_{id}$, while $U_{\ell a}$ is the Pontecorvo–Maki–Nakagawa–Sakata (PMNS) matrix. The short-distance physics is described by the loop functions X_t and X^ℓ , where the dependence on the τ mass introduces a small off-diagonal neutrino coupling, which we ignore in the following. The operator induced in the SM case reads

$$O_{abij}^{A, L} = \frac{1}{2} (\bar{\nu}_{Ma} \gamma_\mu \gamma_5 \nu_{Mb}) (\bar{d}_i \gamma^\mu P_L d_j), \quad O_{abij}^{V, LL} = (\bar{\nu}_{Da} \gamma_\mu P_L \nu_{Db}) (\bar{d}_i \gamma^\mu P_L d_j). \quad (4)$$

in the Majorana and Dirac case, respectively. We have intentionally decided to directly separate the SM from NP contributions in Eq. (1) in order to present the constraints on the NP effects more transparently.

We discuss the dimension-six operator basis for the Majorana and Dirac case in Section 2.1 and Section 2.2, respectively. There are further possibilities, e.g., mixed Dirac–Majorana cases or Dirac masses with lepton-number-violating dimension-six interactions, but as we shall see the main effects can be illustrated within the two aforementioned cases. The basis of operators can be equally well be adjusted by trivial flavour renaming to study $b \rightarrow s/d\nu\nu$ or $c \rightarrow u\nu\nu$ transitions relevant, e.g. for $B \rightarrow K\nu\nu$ or rare charm FCNC with decays to neutrinos.

2.1 Majorana- ν EFT with lepton-number violation

The dimension-six effective Lagrangian relevant for $d_i \rightarrow d_j\nu\nu$ transitions for the case in which all neutrinos are Majorana particles, can be written as

$$\mathcal{L}_{d \rightarrow d'\nu\nu}^{(6)} \Big|_{\text{Majorana}} = \sum_{\substack{I=\{V,A\} \\ \tau=\{L,R\}}} \sum_f C_f^{I,\tau} O_f^{I,\tau} + \left(\sum_{I=\{S,P,T\}} \sum_f C_f^{I,L} O_f^{I,L} + \text{h.c.} \right), \quad (5)$$

where I denotes the type of interaction, $I = \{V, A, S, P, T\}$, which stand for V for vector-, A for axial-vector-, S for scalar-, P for pseudoscalar-, and T for tensor-type interactions. $\tau = \{L, R\}$ indicates the chirality of the quark currents, and f comprises all neutrino and quark flavour indices, $f = \{abij\}$. The full set of independent operators read

$$\begin{aligned} O_{abij}^{V,L} &= \frac{1}{2} (\bar{\nu}_{Ma} \gamma_\mu \nu_{Mb}) (\bar{d}_i \gamma^\mu P_L d_j), & O_{abij}^{V,R} &= \frac{1}{2} (\bar{\nu}_{Ma} \gamma_\mu \nu_{Mb}) (\bar{d}_i \gamma^\mu P_R d_j), \\ O_{abij}^{A,L} &= \frac{1}{2} (\bar{\nu}_{Ma} \gamma_\mu \gamma_5 \nu_{Mb}) (\bar{d}_i \gamma^\mu P_L d_j), & O_{abij}^{A,R} &= \frac{1}{2} (\bar{\nu}_{Ma} \gamma_\mu \gamma_5 \nu_{Mb}) (\bar{d}_i \gamma^\mu P_R d_j), \\ O_{abij}^{S,L} &= \frac{1}{2} (\bar{\nu}_{Ma} \nu_{Mb}) (\bar{d}_i P_L d_j), & O_{abij}^{P,L} &= \frac{1}{2} (\bar{\nu}_{Ma} i\gamma_5 \nu_{Mb}) (\bar{d}_i P_L d_j), \\ O_{abij}^{T,L} &= \frac{1}{2} (\bar{\nu}_{Ma} \sigma_{\mu\nu} \nu_{Mb}) (\bar{d}_i \sigma^{\mu\nu} P_L d_j), \end{aligned} \quad (6)$$

with $i, j = 1, 2, 3$.

Apart from the quark-flavour dependence, the operators $O^{V/A, L/R}$ are self-adjoint after considering standard relations for four-component Majorana fields [30]. This is not the case for the $O^{S/P/T, L}$ operators. We ensure the hermiticity of the Lagrangian by imposing additional conditions on the flavour structure of the Wilson coefficients. The hermiticity condition on the Wilson coefficients $C_f^{V/A, L/R}$ is

$$C_{abij}^{V/A, L/R} = \left(C_{baji}^{V/A, L/R} \right)^*. \quad (7)$$

Additionally, there are the further conditions originating from standard relations specific to four-component Majorana fields [30]

$$C_{abij}^{I,\tau} = \eta C_{baji}^{I,\tau} \quad \text{where} \quad \eta = \begin{cases} +1, & \text{for } I = A, S, P \\ -1, & \text{for } I = V, T. \end{cases} \quad (8)$$

The SM contribution to $K^+ \rightarrow \pi^+ \nu\nu$ ($\bar{s} \rightarrow \bar{d} \nu\nu$ transition) in the Majorana case is induced by the $O_{abij}^{A,L}$ operators with $i = 1$ (down quark) and $j = 2$ (strange quark), as discussed in Eq. (3). Note

that imposing lepton-number conservation forbids the neutrinos mass-term but also the $O^{S/P/T,L}$ interactions, which are thus lepton-number violating.

For $s \rightarrow d\nu\nu$ transitions and the case of three Majorana neutrinos, the number of independent interactions that are symmetric in the flavour of the three Majorana neutrinos are parametrised by $6 \cdot 6$ independent complex Wilson coefficients contained in $C_{ab21}^{A,L/R}$, $C_{ab21}^{S/P,L}$, and $C_{ab12}^{S/P,L}$, with $a \geq b$. In addition, the interactions that are anti-symmetric in the neutrino flavours are parametrised by $3 \cdot 4$ complex Wilson coefficients contained in $C_{ab21}^{V,L}$, $C_{ab21}^{V,R}$, $C_{ab21}^{T,L}$, and $C_{ab12}^{T,L}$, with $a > b$. The same number of 48 independent complex Wilson coefficients contributes to $b \rightarrow s\nu\nu$ decays, after the quark-flavour indices are appropriately changed.

2.2 Dirac- ν EFT with lepton-number conservation

For the case of Dirac neutrinos, the dimension-six effective Lagrangian with lepton-number conservation relevant for $d_i \rightarrow d_j\nu\bar{\nu}$ transitions can be written as

$$\mathcal{L}_{d \rightarrow d'\nu\bar{\nu}}^{(6)} \Big|_{\text{Dirac}} = \sum_{\tau, \tau' = \{L, R\}} \sum_f C_f^{V, \tau\tau'} O_f^{V, \tau\tau'} + \sum_f \left(C_f^{S, LL} O_f^{S, LL} + C_f^{S, LR} O_f^{S, LR} + C_f^{T, LL} O_f^{T, LL} + \text{h.c.} \right), \quad (9)$$

where $\tau, \tau' = \{L, R\}$ indicate the chirality of the neutrino and/or quark currents and f comprises all neutrino and quark flavour indices, $f = \{abij\}$. The independent, lepton-number conserving operators read

$$O_{abij}^{V, LL} = (\bar{\nu}_{Da} \gamma_\mu P_L \nu_{Db}) (\bar{d}_i \gamma^\mu P_L d_j), \quad O_{abij}^{V, LR} = (\bar{\nu}_{Da} \gamma_\mu P_L \nu_{Db}) (\bar{d}_i \gamma^\mu P_R d_j), \quad (10)$$

$$O_{abij}^{V, RL} = (\bar{\nu}_{Da} \gamma_\mu P_R \nu_{Db}) (\bar{d}_i \gamma^\mu P_L d_j), \quad O_{abij}^{V, RR} = (\bar{\nu}_{Da} \gamma_\mu P_R \nu_{Db}) (\bar{d}_i \gamma^\mu P_R d_j), \quad (11)$$

$$O_{abij}^{S, LL} = (\bar{\nu}_{Da} P_L \nu_{Db}) (\bar{d}_i P_L d_j), \quad O_{abij}^{S, LR} = (\bar{\nu}_{Da} P_L \nu_{Db}) (\bar{d}_i P_R d_j), \quad (12)$$

$$O_{abij}^{T, LL} = (\bar{\nu}_{Da} \sigma_{\mu\nu} P_L \nu_{Db}) (\bar{d}_i \sigma^{\mu\nu} P_L d_j). \quad (13)$$

In the Dirac case, the $O^{V, \tau\tau'}$ operators are all self-adjoint if their flavour structure is neglected. The hermiticity condition on their Wilson coefficients reads

$$C_{abij}^{V, \tau\tau'} = \left(C_{baji}^{V, \tau\tau'} \right)^*. \quad (14)$$

In the Dirac basis, the SM contribution to $K^+ \rightarrow \pi^+ \bar{\nu}\nu$ is induced by the operators $O_{abij}^{V, LL}$ with $i = 1$ (down quark) and $j = 2$ (strange quark) and discussed in Eq. (3). In the strict SM case of three massless neutrinos, neutrinos can be described by three left-handed fields without right-handed partners. In this case, the scalar and tensor operators vanish by construction. They do not, however, vanish if the small neutrino masses are due to Dirac masses for which right-handed neutrinos are required. In this case, scalar and tensor interactions are possible *without the need* for lepton-number violation in contrast to the Majorana case.

For $s \rightarrow d\nu\bar{\nu}$ transitions and the case of three Dirac neutrinos, the interactions are parametrised by a total of $9 \cdot 10$ independent complex Wilson coefficients $C_{ab21}^{V, \tau\tau'}$, $C_{ab21}^{S, LL/LR}$, $C_{ab12}^{S, LL/LR}$, $C_{ab21}^{T, LL}$, $C_{ab12}^{T, LL}$, where $\tau, \tau' \in \{L, R\}$. The same number of 90 complex Wilson coefficients contributes to $b \rightarrow s\nu\bar{\nu}$ decays, after the quark flavour indices are appropriately changed.

3 Rates and distributions for $K^+ \rightarrow \pi^+ \nu \bar{\nu}$ at NA62

In this section, we derive the decay rates and the resulting distributions for the decay $K^+ \rightarrow \pi^+ \nu \nu$ for the cases of Majorana and Dirac neutrinos. We also discuss the treatment of theory and experimental uncertainties used throughout the analysis. Finally, we describe the statistical procedure that we shall use to constrain the parameter-space of the effective theories based on current and expected data from NA62 and HIKE, respectively.

3.1 Decay rates

To derive the differential decay rates for $K^+ \rightarrow \pi^+ \nu^{(-)} \bar{\nu}^{(-)}$ we evaluate the matrix element

$$\mathcal{M} = \left\langle \pi^+(p_\pi) \bar{\nu}_a \nu_b^{(-)} \left| H_{\text{eff}} \right| K^+(p_K) \right\rangle ,$$

where the effective Hamiltonian H_{eff} follows either from the Lagrangian in Eq. (6) or from the one in Eq. (10). To be precise, for the Dirac case we compute the amplitude for the transition $K^+ \rightarrow \pi^+ \bar{\nu}_a \nu_b$, while for the Majorana case the one for $K^+ \rightarrow \pi^+ \nu_a \nu_b$. We will mention differences between the Majorana and the Dirac computation when they arise.

The amplitude factorizes into a hadronic part $\langle \pi^+ | O_{sd}^{\text{had}} | K^+ \rangle$ and a leptonic part $\langle \bar{\nu}_a \nu_b | O_{ab}^{\text{lep}} | 0 \rangle$. The leptonic part is obtained using standard techniques; in particular we employ Feynman rules for Majorana fields [31] to treat the case of massive Majorana neutrinos. The hadronic parts of the decay are determined by three form factors [11, 32, 33]

$$\langle \pi^+ | \bar{d} \gamma^\mu s | K^+ \rangle = (p_K + p_\pi)^\mu f^V(q^2) + \frac{m_K^2 - m_\pi^2}{q^2} (p_K - p_\pi)^\mu (f^S(q^2) - f^V(q^2)) , \quad (15)$$

$$\langle \pi^+ | \bar{d} s | K^+ \rangle = \frac{m_K^2 - m_\pi^2}{m_s - m_d} f^S(q^2) , \quad (16)$$

$$\langle \pi^+ | \bar{d} \sigma^{\mu\nu} s | K^+ \rangle = (p_\pi^\mu p_K^\nu - p_\pi^\nu p_K^\mu) \frac{f^T(q^2)}{m_K + m_\pi} , \quad (17)$$

with m_p denoting the masses of mesons and quarks, p_π and p_K the π^+ and K^+ momentum, respectively, and $q^2 \equiv (p_K - p_\pi)^2$. To obtain the tensor form factor, $f^T(q^2)$, we use isospin symmetry to relate it to the neutral form factor, finding $f^T(q^2) = 2f_0^T(q^2)$, with $\langle \pi^0 | \bar{s} \sigma^{\mu\nu} d | K^0 \rangle = (p_\pi^\mu p_K^\nu - p_\pi^\nu p_K^\mu) \sqrt{2} f_0^T(q^2) / (m_K + m_\pi)$ evaluated in Ref. [33]. We drop the subscript “ $K^+ \pi^+$ ” for readability. Note, that the parity violating axial parts of the hadronic matrix elements do not contribute to the decay due to the parity conservation of QCD. The q^2 -dependence of the remnant scalar form-factor functions reads [11, 33]

$$f^V(q^2) = f_0^+ \left(1 + \lambda'_+ \frac{q^2}{m_\pi^2} + \lambda''_+ \frac{q^4}{m_\pi^4} \right) , \quad f^S(q^2) = f_0^+ \left(1 + \lambda_0 \frac{q^2}{m_\pi^2} \right) , \quad f^T(q^2) = \frac{2f_0^T(0)}{1 - \lambda_T q^2} . \quad (18)$$

Table 3.1 contains the numerical input for the form factors. For notational brevity we also define

$$F^S(q^2) \equiv \frac{m_K^2 - m_\pi^2}{m_s - m_d} f^S(q^2) , \quad F^T(q^2) \equiv \frac{f^T(q^2)}{m_K + m_\pi} . \quad (19)$$

The differential partial decay rate for the three-body decay is then given by [18]

$$d\Gamma \left(K^+ \rightarrow \pi^+ \nu^{(-)} \bar{\nu}^{(-)} \right) = \frac{(2\pi)^4}{2E_K} |\mathcal{M}|^2 \frac{d^3 \vec{p}_\pi}{(2\pi)^3 E_\pi} \frac{d^3 \vec{p}_{\nu,a}}{(2\pi)^3 E_{\nu,a}} \frac{d^3 \vec{p}_{\nu,b}}{(2\pi)^3 E_{\nu,b}} , \quad (20)$$

Table 1: Numerical values of the form factor parameters used. The values for the scalar and vector form factor are taken from Ref. [11, 32], while the parameters of the tensor form factor are taken from Ref. [33].

Form factor	Parameters
f_S	$f_0^+ = 0.9778$ $\lambda_0 = (13.38 \pm 1.19) \cdot 10^{-3}$
f_V	$f_0^+ = 0.9778$ $\lambda'_+ = (24.82 \pm 1.10) \cdot 10^{-3}$ $\lambda''_+ = (1.64 \pm 0.44) \cdot 10^{-3}$
f_T	$f_0^T = 0.417(14_{\text{stat}})(5_{\text{syst}})$ $s_T = 1.10(8_{\text{stat}})(11_{\text{syst}}) \text{ GeV}^{-2}$

where $|\overline{\mathcal{M}}|$ indicates that we have summed over the polarisations of the final-state neutrinos. Starting from this equation, one can derive the differential distribution $d^2\Gamma_{ab}/dq^2 dk^2$ in terms of the Lorentz invariant parameters $q^2 \equiv (p_{\nu,a} + p_{\nu,b})^2$ and $k^2 \equiv (p_\pi + p_{\nu,a})^2$ to obtain the characteristic for three-body decays Dalitz plot. The corresponding expressions in the Majorana and Dirac case are provided in Appendix A.

However, NA62 measures the differential branching ratio $d\text{Br}/d|\vec{p}_\pi|$ in the lab frame. To arrive at this expression, we recursively write the three-body phase-space integration into a convolution of two two-particle phase-space integrations. This introduces an additional integration over the variable $q^2 = (p_{\nu,a} + p_{\nu,b})^2$ but allows one to trivially perform the integration over both neutrino momenta. After the integration over the angular part of the pion momentum in the lab frame, we are left with the double differential decay rate $d^2\Gamma_{ab}/d|\vec{p}_\pi|dq^2$ in the lab frame.

For the case of a decay to two massless neutrinos, ν_a and ν_b , the double differential partial decay width of $K^+ \rightarrow \pi^+ \nu_a \nu_b$ in the Majorana basis then reads

$$\begin{aligned}
\left. \frac{d^2\Gamma_{ab}}{d|\vec{p}_\pi|dq^2} \right|_{\text{Majorana}} &= \frac{|\vec{p}_\pi|}{6144\pi^3 E_K E_\pi |\vec{p}_K| (1 + \delta_{ab})} \Theta(|\vec{p}_\pi|, q^2) \Big|_{m_a=m_b=0} \left[\right. \\
&\quad + 8\lambda_{K\pi q^2} |f^V(q^2)|^2 \left(\left| C_{ab12}^{A,L,\text{SM}} + C_{ab12}^{A,L} + C_{ab12}^{A,R} \right|^2 + \left| C_{ab12}^{V,L} + C_{ab12}^{V,R} \right|^2 \right) \\
&\quad + 12q^2 |F^S(q^2)|^2 \left(\left| C_{ab12}^{P,L} + C_{ab21}^{P,L*} \right|^2 + \left| C_{ab12}^{S,L} + C_{ab21}^{S,L*} \right|^2 \right) \\
&\quad \left. + 3q^2 \lambda_{K\pi q^2} |F^T(q^2)|^2 \left(\left| C_{ab12}^{T,L} - C_{ab21}^{T,L*} \right|^2 \right) \right] \quad (21)
\end{aligned}$$

with $\lambda_{K\pi q^2} \equiv \lambda(m_K^2, m_\pi^2, q^2)$ and the Källén function $\lambda(x, y, z) \equiv x^2 + y^2 + z^2 - 2xy - 2yz - 2zx$. The additional factor $1/(1 + \delta_{ab})$ accounts for the reduction of the phase space in the case of identical particles in the final state. We stress that in Eq. (21) we have already used the hermiticity and Majorana conditions to obtain all contributions to the neutrino final state $\nu_a \nu_b$. Therefore, the total rate corresponds to the “constrained” sum of channels $\sum_{a \leq b}$ of all independent final states. In Eq. (21),

$\Theta(|\vec{p}_\pi|, q^2)$ is a shorthand for the theta-functions

$$\begin{aligned} \Theta(|\vec{p}_\pi|, q^2) &\equiv \theta(E_K - E_\pi) \theta(\sqrt{q^2} - m_a - m_b) \\ &\times \theta\left(1 - \frac{m_K^2 + m_\pi^2 - 2E_K E_\pi - q^2}{2|\vec{p}_K||\vec{p}_\pi|}\right) \theta\left(1 + \frac{m_K^2 + m_\pi^2 - 2E_K E_\pi - q^2}{2|\vec{p}_K||\vec{p}_\pi|}\right). \end{aligned} \quad (22)$$

Analogously, we compute the differential partial decay width of $K^+ \rightarrow \pi^+ \bar{\nu}_a \nu_b$ for the massless Dirac-neutrino case

$$\begin{aligned} \left. \frac{d^2 \Gamma_{ab}}{d|\vec{p}_\pi| dq^2} \right|_{\text{Dirac}} &= \frac{|\vec{p}_\pi|}{3072\pi^3 E_K E_\pi |\vec{p}_K|} \Theta(|\vec{p}_\pi|, q^2) \Big|_{m_a=m_b=0} \left[\right. \\ &+ 2\lambda_{K\pi q^2} |f^V(q^2)|^2 \left(|C_{ab12}^{V,LL,SM} + C_{ab12}^{V,LL} + C_{ab12}^{V,LR}|^2 + |C_{ab12}^{V,RL} + C_{ab12}^{V,RR}|^2 \right) \\ &+ 3q^2 |F^S(q^2)|^2 \left(|C_{ab12}^{S,LL} + C_{ab12}^{S,LR}|^2 + |C_{ba21}^{S,LL} + C_{ba21}^{S,LR}|^2 \right) \\ &\left. + q^2 \lambda_{K\pi q^2} |F^T(q^2)|^2 \left(|C_{ab12}^{T,LL}|^2 + |C_{ba21}^{T,LL}|^2 \right) \right] \end{aligned} \quad (23)$$

Similarly to the Majorana case, also here we have used the hermiticity conditions on the Wilson coefficients in order to include all contributions to the $\bar{\nu}_a \nu_b$ final state. However, contrarily to the Majorana case, particles are not the same as antiparticles and thus the total rate is given by the unconstrained sum of channels $\sum_{a,b}$.

The total branching ratio for $K^+ \rightarrow \pi^+ \nu \bar{\nu}^{(-)}$ is then the sum of the different neutrino channels

$$\text{Br}\left(K^+ \rightarrow \pi^+ \nu \bar{\nu}^{(-)}\right) = \Gamma_{\text{tot}}^{-1} \int_{\Omega(|\vec{p}_\pi|, q^2)} d|\vec{p}_\pi| dq^2 \sum_{a,b} \overline{\frac{d^2 \Gamma_{ab}}{d|\vec{p}_\pi| dq^2}}, \quad (24)$$

where $\Omega(|\vec{p}_\pi|, q^2)$ denotes the signal region of the NA62 experiment, Γ_{tot} the total decay width in the lab frame, and the overline in \sum indicates that for the Majorana case the sum is constrained, i.e., $a \leq b$, while for the Dirac case it is unconstrained.

Uncertainties in theory predictions

There are two main sources of uncertainties in the theory predictions for the $K \rightarrow \pi \nu \nu$ rates and distributions: (i) uncertainties associated to the SM Wilson coefficient and (ii) uncertainties associated to the form-factors.

For (i), i.e., SM Wilson coefficient, we follow Ref. [17]. We include all state-of-the-art perturbative corrections and include in our analysis both pure theory uncertainties, associated to residual scale dependencies, and parametric uncertainties. At the current level of precision, the dominant uncertainties are parametric, mainly originating from the CKM input. All these uncertainties are due to short-distance dynamics and thus do not depend on q^2 .

For (ii), i.e., the form factors, we use their numerical values and uncertainties as published in the original literature and summarised in Table 3.1. The numerical evaluation of the form factors shows that their relative uncertainties are roughly constant within the q^2 signal regions of NA62. This is illustrated in Figure 3.1, where we show the q^2 dependence of the three form-factor functions and their uncertainties in the NA62 signal regions. The lower panel shows the q^2 dependence of their

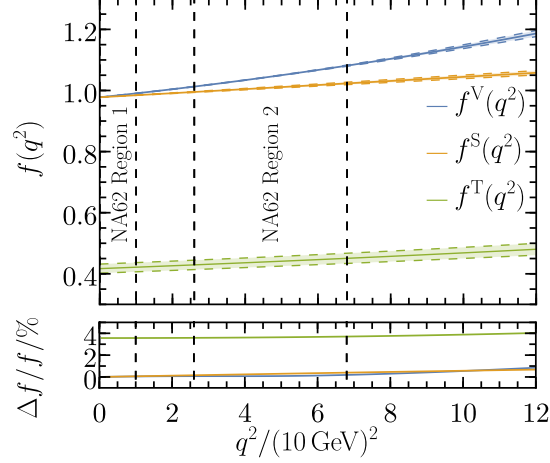


Figure 1: The q^2 dependence of the form-factor functions and their uncertainties as given in Table 3.1. The coloured bands correspond to the 1σ bands for the vector, scalar and tensor form-factors. The lower panel shows the dependence of the relative uncertainty $\Delta f/f$ of each form-factor function.

relative uncertainties $\Delta f/f$. Since these uncertainties are roughly flat in q^2 , we can consider them as global relative uncertainties, which speeds up the evaluation of the profile likelihood ratio test. This simplifies accounting for them in the likelihood evaluation. Concretely, we use throughout the whole signal region an overall relative error of 0.4%, 0.8%, and 4% for the vector, scalar, and tensor form factor, respectively, cf., Figure 3.1.

3.2 Statistical treatment for EFT fit

To quantify the agreement between the experimental data and the different NP scenarios, we perform a statistical test using a profile likelihood ratio as test statistic that is sampled in a full frequentist manner. The number of signal events, s_i , in a category i is given as

$$s_i = \frac{\text{BR}_{K \rightarrow \pi \nu \nu}^i(\{C_{\text{NP}}\})}{\text{SES}_i}, \quad (25)$$

where $\text{BR}_{K \rightarrow \pi \nu \nu}^i(\{C_{\text{NP}}\})$ denotes the branching ratio of $K^+ \rightarrow \pi^+ \nu \nu$ within the category i for a set of Wilson coefficients $\{C_{\text{NP}}\}$ corresponding to the NP scenario under consideration. Further, the variable SES_i denotes the single-event sensitivity of category i taken from Ref. [34]. Note that in Ref. [2, 34], the SES_i are defined such that multiplied with the total branching ratio one obtains the number of expected events in bin i . This is in contrast to our definition in Eq. (25) where we use the branching ratio within the corresponding categories. We, thus, remove the phase-space information from the original definition of the SES_i , cf. Table 2.

The number of expected background events, b_i , and observed data, n_i , in each category are taken from the NA62 measurement [2]. The events in the different categories are uncorrelated, which implies that the total likelihood is a product of Poisson distributions in the number of signal plus background events $s_i + b_i$. We further neglect possible correlations between experimental parameters like the SES_i , which—if non-zero—are not provided by the NA62 collaboration. We account for theory and experimental statistical uncertainties in the likelihood by including the corresponding parameters as global observables associated to auxiliary measurements. The uncertainties of the parameters for

Table 2: The single-event sensitivities, SES_i , for the respective categories provided by the NA62 collaboration [1, 2, 34, 35], as well as the corresponding sensitivities with the phase-space information removed. The definition of each category is given in the original NA62 publications.

Category	0	1	2	3	4	5	6	7	8
$\text{SES}/10^{-10}$ from [1, 2, 34, 35]	3.15	0.39	0.54	1.48	0.59	0.55	0.63	1.22	1.75
$\text{SES}/10^{-12}$ w/o kinematic cuts	76.01	8.45	16.03	8.04	3.20	2.99	3.42	4.86	6.97

the theory predictions described in Section 3.1 are all assumed to be Gaussian even though some of them, e.g., scale dependencies are of non-statistical nature. However, the numerical impact of this assumption on the analysis is negligible. The sensitivities, SES_i , are constrained to follow uncorrelated Gaussian terms while the number of expected background events follows a Poisson distribution.

Let us now denote the total likelihood with the shorthand notation $\mathcal{L}(x|\{C_{\text{NP}}\}, \nu)$, with x being the outcome, i.e., the observed data, $\{C_{\text{NP}}\}$ the parameters of interest, i.e., the NP Wilson coefficients, and ν the nuisance parameters. Under the assumption that the NP scenario under consideration is realised in nature, one can determine the confidence intervals on the model parameters $\{C_{\text{NP}}\}$ at a given confidence level using the profile likelihood ratio λ as a test statistic

$$\lambda_{\{C_{\text{NP}}\}} = \frac{\mathcal{L}(x|\{C_{\text{NP}}\}, \hat{\nu}(\{C_{\text{NP}}\}))}{\mathcal{L}(x|\{\hat{C}_{\text{NP}}\}, \hat{\nu})}. \quad (26)$$

The parameters with a single hat are the parameter values that maximise the likelihood. The value for the nuisance parameters ν that maximise the likelihood for given values of the parameters of interest $\{C_{\text{NP}}\}$ are denoted with a double-hat. For given parameters of interest $\{C_{\text{NP}}\}$, we calculate the corresponding p -value via

$$p_{\{C_{\text{NP}}\}} = \int_{\lambda_{\{C_{\text{NP}}\}}^{\text{obs}}}^{\infty} d\lambda_{\{C_{\text{NP}}\}} f(\lambda_{\{C_{\text{NP}}\}}|\{C_{\text{NP}}\}, \nu), \quad (27)$$

where f denotes the test-statistic distribution that we sample by means of a Monte-Carlo method under the assumption of $\{C_{\text{NP}}\}$, and with $\lambda_{\{C_{\text{NP}}\}}^{\text{obs}}$ the observed value of the test statistic. In order to determine the upper limit on a single Wilson coefficient C_{NP} at a confidence level of $100(1 - \alpha)\%$, we solve for $p_{C_{\text{NP}}} = \alpha$. For the procedure on how to estimate two-dimensional confidence regions from the profile likelihood ratio see, e.g., Ref. [36]. For further references, see Refs. [18, 37]

4 New Physics sensitivities

In this Section, we use the NP distributions from Section 3.1 together with the binned likelihood from Section 3.2 to determine NA62's sensitivity on constraining the independent NP operators given in Section 2.1 and 2.2 for Majorana and Dirac neutrinos, respectively. We shall discuss the sensitivity based on the current experimental data of NA62 [2] and also provide estimates for the future sensitivity based on the prospects in future experiments like HIKE. In Section 4.1 we switch on one NP operator at a time, while in Section 4.2 we also show correlations by switching on pairs of operators. The limits on all Wilson coefficients are always determined in addition to the Standard Model contribution, which is always included.

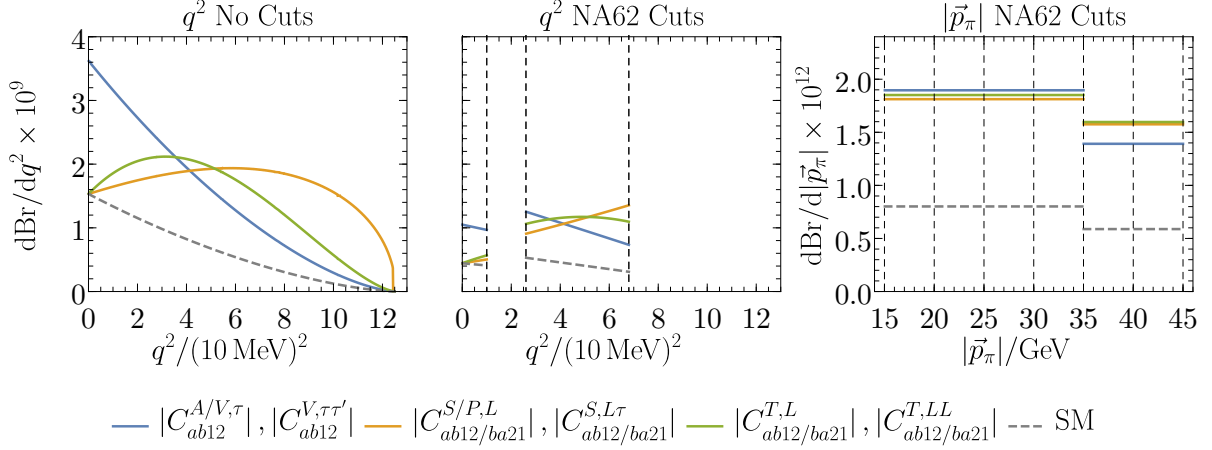


Figure 2: Distributions of $\text{Br}(K^+ \rightarrow \pi^+ \nu \nu)$ for different NP scenarios containing three massless Majorana or Dirac neutrinos. The left and middle panel shows differential q^2 distributions integrated over the whole physical phase space for $|\vec{p}_\pi|$ and over $|\vec{p}_\pi|$ signal region of NA62, respectively. The right panel shows the lab frame $|\vec{p}_\pi|$ distribution inside the NA62 q^2 signal regions as currently done at NA62. All NP Wilson coefficients that affect the rates are displayed in the legend. In each panel we use the values for the given Wilson coefficients that saturate the bound at 90% CL. Therefore, there is no distinction between $a = b$ and $a \neq b$ cases. The gray, dashed line corresponds to the SM case. The dashed, vertical lines indicate the different NA62 signal regions.

4.1 Single-operator fits

For the single-operator fits we discuss three different scenarios:

- (i) Dirac effective theory with three light neutrinos, i.e., $a, b = 1, 2, 3$ with $m_{\nu,1} \approx m_{\nu,2} \approx m_{\nu,3} \approx 0$ (operator basis of Section 2.2).
- (ii) Majorana effective theory with three light neutrinos, i.e., $a, b = 1, 2, 3$ with $m_{\nu,1} \approx m_{\nu,2} \approx m_{\nu,3} \approx 0$ (operator basis of Section 2.1).
- (iii) Majorana effective theory with three light neutrinos and one additional sterile neutrino with mass $m_{\nu,4}$, i.e., $a, b = 1, 2, 3, 4$, (operator basis of Section 2.1).

Since in this Section we switch on one operator at a time, the bounds are only sensitive to the absolute value of the respective Wilson coefficients and insensitive to their CP violating phases. The exceptions are NP contributions that induce the same operator as the SM, i.e., $O_{aa12}^{A,L}$ and $O_{aa12}^{V,LL}$, for which the interference term with the SM depends on the relative phase between the NP and the SM Wilson coefficient. Since $K^+ \rightarrow \pi^+ \nu \nu$ is a CP conserving decay we choose for concreteness to align the NP with SM phase in the numerical analysis that follows.

Even though the cases (i) and (ii) are physically distinguishable due to the different number of degrees of freedom there will always be a scenario in (i) that leads to the same NP distribution as a scenario in (ii) in the limit of $m_\nu \rightarrow 0$ if a single NP operator is switched on. This is best seen by comparing the Majorana to the Dirac distributions for massless neutrinos in Eqs. (21) and (23) and is illustrated also in Figure 2, where we present all the independent differential distributions possible for the case (i) and (ii). Throughout Figure 2, the value of the Wilson coefficients is chosen to saturate

Table 3: Current and estimated future experimental lower limit at 90% CL for the different NP operators in the case of three massless Majorana neutrinos. A single operator is turned on at a time. The case labelled by $\sum a = b$ corresponds to taking neutrino-flavour universal Wilson coefficients, whereas in the case labelled by $a = b$ a single Wilson coefficient is switched on. Note that in case of interference with the SM Wilson coefficient, the CP phase of the NP Wilson coefficient has been aligned to the SM. See text for the details on the different future scenarios.

ν -Majorana EFT		current	future	future[q^2 bins]
$1/\sqrt{ C_{ab12}^{V,L/R} }$	$a \neq b$	$7.6 \cdot 10^1$ TeV	$1.2 \cdot 10^2$ TeV	$1.2 \cdot 10^2$ TeV
$1/\sqrt{ C_{ab12}^{A,L/R} }$	$\sum a = b$	$1.2 \cdot 10^2$ TeV	$2.8 \cdot 10^2$ TeV	$2.6 \cdot 10^2$ TeV
	$a = b$	$8.1 \cdot 10^1$ TeV	$1.7 \cdot 10^2$ TeV	$1.6 \cdot 10^2$ TeV
	$a \neq b$	$7.6 \cdot 10^1$ TeV	$1.2 \cdot 10^2$ TeV	$1.2 \cdot 10^2$ TeV
$1/\sqrt{ C_{ab12/21}^{S,L} }$	$\sum a = b$	$1.6 \cdot 10^2$ TeV	$2.4 \cdot 10^2$ TeV	$2.5 \cdot 10^2$ TeV
	$a = b$	$1.2 \cdot 10^2$ TeV	$1.9 \cdot 10^2$ TeV	$1.9 \cdot 10^2$ TeV
	$a \neq b$	$1.4 \cdot 10^2$ TeV	$2.2 \cdot 10^2$ TeV	$2.3 \cdot 10^2$ TeV
$1/\sqrt{ C_{ab12/21}^{P,L} }$	$\sum a = b$	$1.6 \cdot 10^2$ TeV	$2.4 \cdot 10^2$ TeV	$2.5 \cdot 10^2$ TeV
	$a = b$	$1.2 \cdot 10^2$ TeV	$1.9 \cdot 10^2$ TeV	$1.9 \cdot 10^2$ TeV
	$a \neq b$	$1.4 \cdot 10^2$ TeV	$2.2 \cdot 10^2$ TeV	$2.3 \cdot 10^2$ TeV
$1/\sqrt{ C_{ab12/21}^{T,L} }$	$a \neq b$	$3.0 \cdot 10^1$ TeV	$4.7 \cdot 10^1$ TeV	$4.7 \cdot 10^1$ TeV

the current experimental limit at 90% Confidence Level (CL). The limits are determined from the prescription of Section 3.2.

In the left panel and middle panel of Figure 2, we show the different $d\text{Br}(K^+ \rightarrow \pi^+ \nu \nu)/d q^2$ distributions. The difference between left and middle panel is that the former shows the distributions integrated over the whole pion-momentum, $|\vec{p}_\pi|$, phase space while in the latter we have integrated over the pion-momentum signal region of NA62. A comparison of the different shapes shows how a differential measurement can be used to distinguish different operators. The right panel shows the distributions $d\text{Br}(K^+ \rightarrow \pi^+ \nu \nu)/d|\vec{p}_\pi|$ in the NA62 lab frame after integrating over the q^2 signal region of NA62. This corresponds exactly to the categories 3–8 currently employed by NA62 [2]. This plot also makes it evident that a binning in the missing-momentum square, q^2 , is able to distinguish between the different NP scenarios within the Majorana or the Dirac basis but not between the Majorana or Dirac nature of the neutrinos. In Table 3 and 4 we collect the constraints at 90% CL on the different Wilson coefficients for the case of three Majorana neutrinos, i.e., scenario (i), and three Dirac neutrinos, i.e., scenario (ii), respectively.

Additionally, we perform first estimates of the future sensitivity reach based on the proposed HIKE experiment. To this end we use the expected improvements highlighted in the letter of intent for HIKE [19, 38] and perform a naive upscaling of the luminosity such that the expected number of signal events reach 400–500 while also reducing the number of background events to ensure that the intended signal to background ratio of $B/S \sim 0.5$ – 0.7 is achieved.¹ Apart from this, we assume the same experimental setup as NA62. We take the expected data to be the sum of the expected SM contribution

¹Ref. [19] and private communication with NA62.

Table 4: Current and estimated future experimental lower limit at 90% CL for the different NP operators in the case of three massless Dirac neutrinos. A single operator is turned on at a time. The case labelled by $\sum a = b$ corresponds to taking neutrino-flavour universal Wilson coefficients, whereas in the case labelled by $a = b$ a single Wilson coefficient is switched on. Note that in case of interference with the SM Wilson coefficient, the CP phase of the NP Wilson coefficient has been aligned to the SM. See text for the details on the different future scenarios.

ν -Dirac EFT		current	future	future[q^2 bins]
$1/\sqrt{ C_{ab12}^{V,L\tau} }$	$\sum a = b$	$1.2 \cdot 10^2$ TeV	$2.8 \cdot 10^2$ TeV	$2.6 \cdot 10^2$ TeV
	$a = b$	$8.2 \cdot 10^1$ TeV	$1.7 \cdot 10^2$ TeV	$1.6 \cdot 10^2$ TeV
	$a \neq b$	$6.3 \cdot 10^1$ TeV	$1.0 \cdot 10^2$ TeV	$9.6 \cdot 10^1$ TeV
$1/\sqrt{ C_{ab12}^{V,R\tau} }$	$\sum a = b$	$8.4 \cdot 10^1$ TeV	$1.3 \cdot 10^2$ TeV	$1.3 \cdot 10^2$ TeV
	$a = b$	$6.3 \cdot 10^1$ TeV	$1.0 \cdot 10^2$ TeV	$9.6 \cdot 10^1$ TeV
	$a \neq b$	$6.3 \cdot 10^1$ TeV	$1.0 \cdot 10^2$ TeV	$9.6 \cdot 10^1$ TeV
$1/\sqrt{ C_{ab12/21}^{S,L\tau} }$	$\sum a = b$	$1.6 \cdot 10^2$ TeV	$2.5 \cdot 10^2$ TeV	$2.5 \cdot 10^2$ TeV
	$a = b$	$1.2 \cdot 10^2$ TeV	$1.9 \cdot 10^2$ TeV	$1.9 \cdot 10^2$ TeV
	$a \neq b$	$1.2 \cdot 10^2$ TeV	$1.9 \cdot 10^2$ TeV	$1.9 \cdot 10^2$ TeV
$1/\sqrt{ C_{ab12/21}^{T,LL} }$	$\sum a = b$	$3.5 \cdot 10^1$ TeV	$5.7 \cdot 10^1$ TeV	$5.7 \cdot 10^1$ TeV
	$a = b$	$2.7 \cdot 10^1$ TeV	$4.2 \cdot 10^1$ TeV	$4.2 \cdot 10^1$ TeV
	$a \neq b$	$2.7 \cdot 10^1$ TeV	$4.2 \cdot 10^1$ TeV	$4.2 \cdot 10^1$ TeV

plus the upscaled background of NA62 after the aforementioned reduction. The resulting limits are shown in the column labeled “future” in Table 3 and 4 for the Majorana and Dirac case, respectively.

For the NP scenarios (i) and (ii), we also estimate the expected limits on the Wilson coefficients by choosing an alternative categorisation of the events. For this we integrate over pion-momentum signal region, but choose to bin the data in the current low- q^2 and high- q^2 signal region NA62 in two and four equidistant q^2 -bins, respectively. To achieve this, we rescale the SES of the 2018-NEWCOL sample (category 3-8) under the assumption that the efficiencies entering the SES and the background distributions are flat in q^2 . The expected data is taken to be the sum of the expected SM contribution plus the upscaled background. The estimated sensitivities to the NP operators are shown in the right column of Table 3 and 4 for the Majorana and Dirac case, respectively. In both future scenarios, we observe an increase of approximately 50%–60% for all NP operators apart from the diagonal vector ones that interfere with the Standard Model. For them we observe an increase in sensitivity of 100%–130%.

Finally, in the context of single-operator fits we also study scenario (iii). Namely, the case of having a fourth massive Majorana neutrino, ν_4 , with a mass such that the decays $K^+ \rightarrow \pi^+ \nu \nu_4$ or $K^+ \rightarrow \pi^+ \nu_4 \nu_4$ are kinematically possible. To illustrate the possible impact of a fourth massive neutrino on the distributions we choose the benchmark mass $m_{\nu_4} = 50$ MeV and show in Figure 3 the analogous distributions as for the three massless neutrino cases.

Figure 4 shows the current constraints at 90% CL as a function of the fourth neutrino mass m_{ν_4} . The left panel shows the current sensitivity while the right one the projected sensitivity. All limits are given at 90% CL. Here we observe an increase of 50%–60% in the sensitivities depending on the NP operator. Note that the kinematic endpoint of the contribution of the diagonal operators, i.e., $O_{4412/21}^{S/P,L}$ and $O_{4412}^{A,L/R}$ (dashed lines), lies at around ~ 130 MeV as the final state necessarily contains

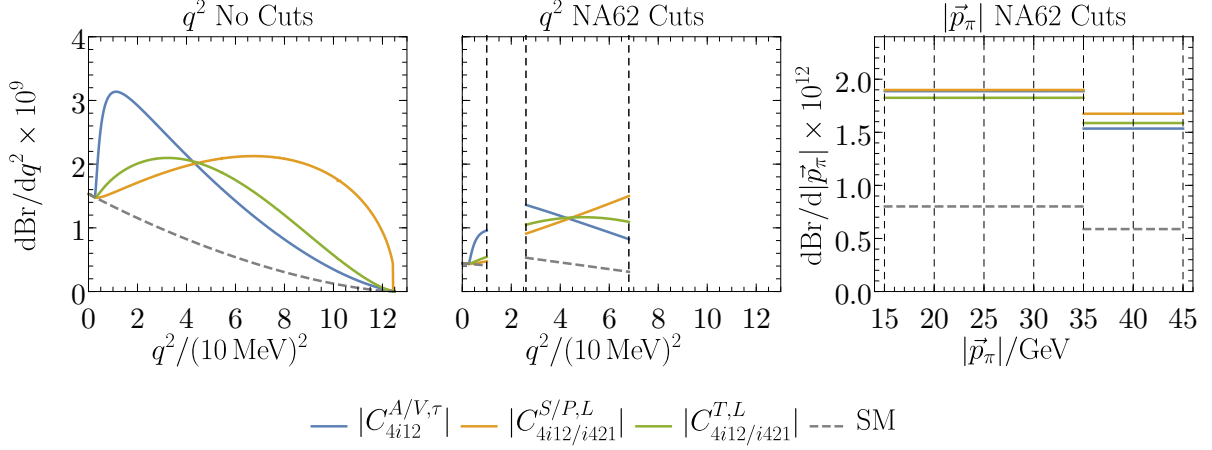


Figure 3: Distributions of $\text{Br}(K^+ \rightarrow \pi^+ \nu \nu)$ for different NP scenarios containing an additional fourth massive Majorana neutrino with mass, $m_{\nu,4} = 50 \text{ MeV}$. Similarly to Figure 2, the left and middle panel shows differential q^2 distributions integrated over the whole physical phase space for $|\vec{p}_\pi|$ and over the $|\vec{p}_\pi|$ signal region of NA62, respectively. The right panel shows the lab frame $|\vec{p}_\pi|$ distribution inside the NA62 q^2 signal regions as currently done at NA62. All NP Wilson coefficients that affect the rates are displayed in the legend. In each panel we use the values for the given Wilson coefficients that saturate the bound at 90% CL. The gray, dashed line corresponds to the SM case. The dashed, vertical lines indicate the different NA62 signal regions.

two massive neutrinos.

4.2 Multi-operator correlations

Next we study the correlations of probing different operators by considering the effect of switching on pairs of different operators simultaneously. For concreteness we cover (almost) all different non-trivial combinations for the case of three massless Dirac or Majorana neutrinos, scenario (i) and (ii), respectively. For these correlations it can be important to specify the phase we chose for the NP Wilson coefficients, since relative phases can be relevant for interferences. We assume there is no new CP-violating phases beyond the SM, i.e., all NP phases are aligned to the SM one. Additionally, in the discussion of neutrino-flavour diagonal operators, e.g., $O_{aa12}^{V,LL}$, we consider the flavour-universal case in which we switch on all operators of the category simultaneously but with universal Wilson coefficients, e.g., $C_{1112}^{V,LL} = C_{2212}^{V,LL} = C_{3312}^{V,LL}$. This additional assumption of flavour universality reduces the number of different combinations.

The results are shown in Figure 5 and 6. For each case we determine the allowed region at 68% CL (dark blue region) and 90% CL (light blue region) in the plane of two Wilson coefficients assuming that the NP scenario is realised in nature. The dashed, black lines correspond to the 90% CL future projection.

5 Discussion and conclusions

The golden, rare kaon decays $K \rightarrow \pi \nu \nu$ provide an excellent test of the Standard Model and are already placing stringent constraints on the parameter space of New Physics. The expected and

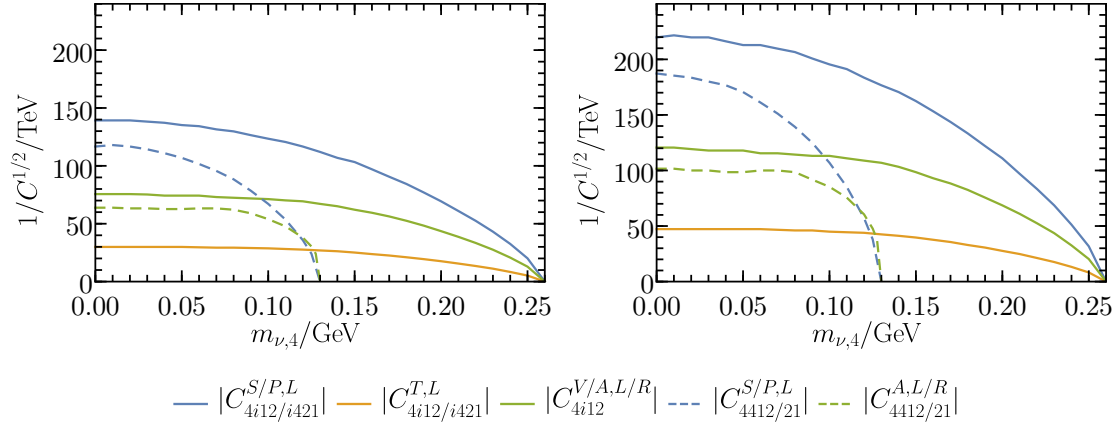


Figure 4: Current (left) and future (right) lower limits of $1/\sqrt{C}$ at 90% CL for the scenarios with an additional massive fourth neutrino interacting solely via one of the given NP Wilson coefficients as a function of its mass $m_{\nu,4}$.

planned experimental activities will test modifications of the SM operators at energies of $\mathcal{O}(300 \text{ TeV})$ and will also allow to extract additional information from the invariant mass spectrum of the neutrinos. In the weak effective theory, scalar and tensor operators induce a modified invisible mass distribution, c.f. Figure 3.1. We have classified all independent Majorana and Dirac operators that contribute to these FCNC decays to neutrinos. We have derived the sensitivity to each operator for the current and expected future experimental situation including experimental and theoretical uncertainties, see Tables 3 and 4. The expected constraints on the NP scale range from $\mathcal{O}(40 \text{ TeV})$ for tensor operators to $\mathcal{O}(300 \text{ TeV})$ for axial-vector Majorana and vector Dirac operators. We have studied the impact of a massive sterile neutrino on the invisible mass spectrum and have discussed the correlation of various operators by analysing the allowed parameter space for pairs of different NP operators.

Majorana and Dirac neutrinos, which can be generated from a lepton-number violating SMEFT or a lepton-number conserving ν SMEFT theory with additional right-handed neutrinos, have a completely different UV origin. Therefore, the relevant weak effective theories also contain different number of independent parameters. This implies that concrete UV models could be tested from the data of the spectrum in future searches. The NP sensitivity of the invisible spectrum provides a strong motivation for the future Kaon program and we plan to study the discriminating power of the charged decay mode spectrum on different realisations of the SMEFT and ν SMEFT in the future [39].

Acknowledgments

We thank Radoslav Marchevski for the discussion regarding the future prospects of the HIKE experiment. Moldanazarova Ulserik was supported by the grant AP14972893 from the Committee of Science of the Ministry of Science and Higher Education of the Republic of Kazakhstan. The work of MG is partially supported by the UK Science and Technology Facilities Council grant ST/X000699/1. UM and MG thanks the particle theory group at the TU Dortmund for the hospitality during the time in which this work was in part done.

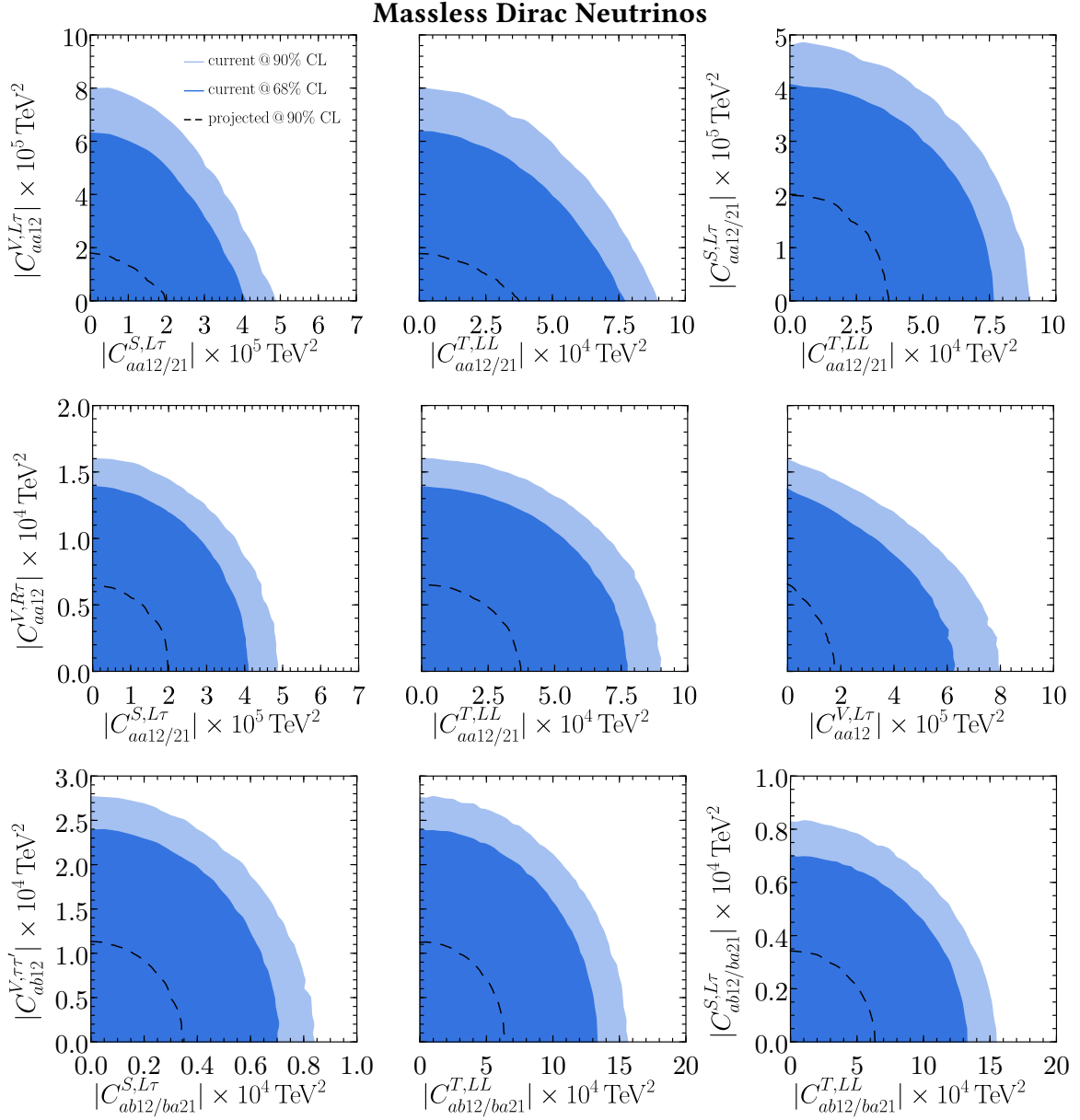


Figure 5: Allowed parameter space at 68% CL (dark blue) and 90% CL (light blue) in the plane of two NP Wilson coefficients corresponding to various combinations of scenario (i), i.e. the case of three massless Dirac neutrinos. Note that here $a \neq b$. The dashed line corresponds to the future projection for the HIKE experiment at 90% CL.

Massless Majorana Neutrinos

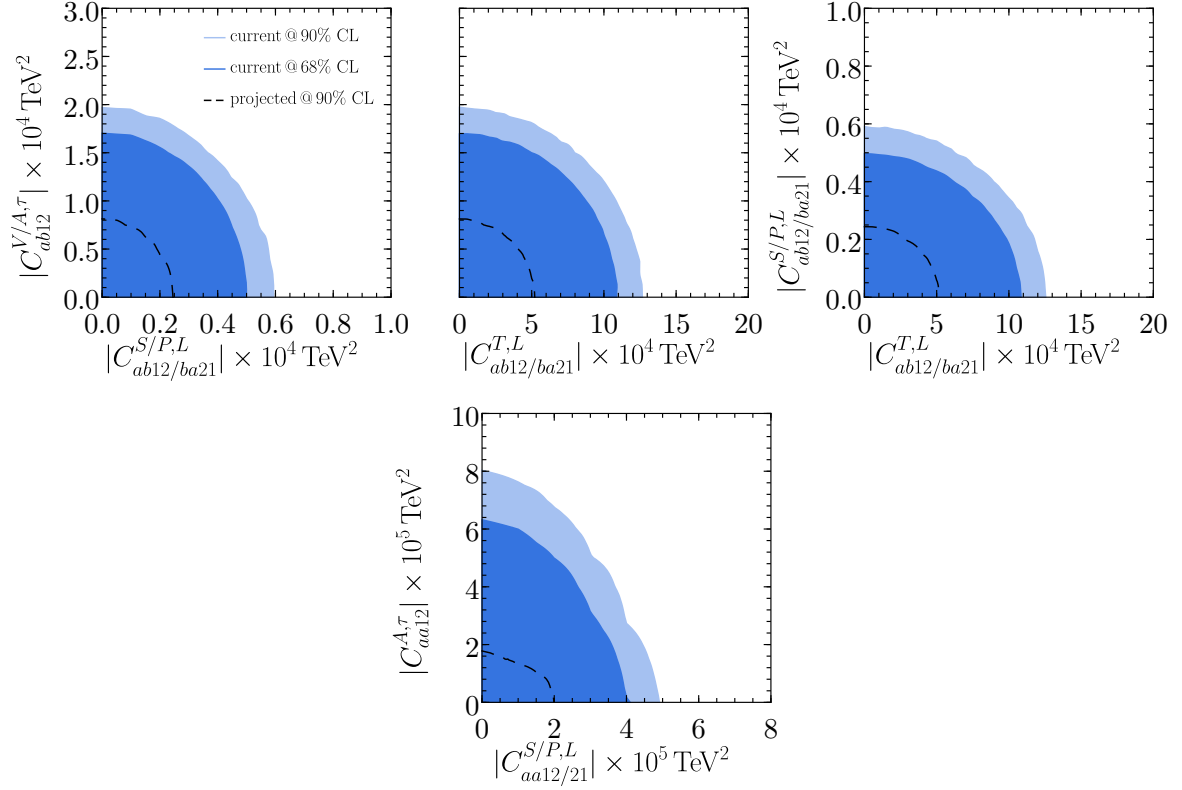


Figure 6: Allowed parameter space at 68% CL (dark blue) and 90% CL (light blue) in the plane of two NP Wilson coefficients corresponding to various combinations of scenario (ii), i.e. the case of three massless Majorana neutrinos. Note that here $a \neq b$. The dashed line corresponds to the future projection for the HIKE experiment at 90% CL.

A Decay rates

The full expressions for the double differential decay widths $d^2\Gamma_{ab}/dq^2 d|\vec{p}_\pi|$ and $d^2\Gamma_{ab}/dq^2 dk^2$ for massive Majorana and Dirac neutrinos are openly available in a git repository on GitLab [40]. Here we give expressions for the double differential partial decay width in terms of the Lorentz invariant Dalitz variables $q^2 = (p_K - p_\pi)^2$ and $k^2 = (p_\pi + p_{\nu,a})^2$ for massless neutrinos. In the Majorana case we find

$$\begin{aligned}
\left. \frac{d^2\Gamma_{ab}}{dq^2 dk^2} \right|_{\text{Majorana}} = & \frac{1}{512\pi^3 m_K^3 (1 + \delta_{ab})} \Theta_{\text{L. inv.}}(q^2, k^2) \Big|_{m_a=m_b=0} \left[\right. \\
& - 4 |f^V(q^2)|^2 (k^4 - k^2(m_K^2 + m_\pi^2 - q^2) + m_K^2 m_\pi^2) \\
& \times \left(|C_{ab12}^{A,L,\text{SM}} + C_{ab12}^{A,L} + C_{ab12}^{A,R}|^2 + |C_{ab12}^{V,L} + C_{ab12}^{V,R}|^2 \right) \\
& + q^2 |F^S(q^2)|^2 \left(|C_{ab12}^{P,L} + C_{ab21}^{P,L*}|^2 + |C_{ab12}^{S,L} + C_{ab21}^{S,L*}|^2 \right) \\
& + q^2 |F^T(q^2)|^2 (-2k^2 + m_K^2 + m_\pi^2 - q^2)^2 \left(|C_{ab12}^{T,L} - C_{ab21}^{T,L*}|^2 \right) \\
& + 2q^2 (2k^2 - m_K^2 - m_\pi^2 + q^2) \left(\right. \\
& \quad - F^S(q^2) F^T(q^2) \text{Im} \left(C_{ab12}^{S,L} C_{ab21}^{T,L} + C_{ab21}^{S,L} C_{ab12}^{T,L} \right) \\
& \quad \left. + F^S(q^2) (F^T(q^2))^* \text{Im} \left(C_{ab21}^{S,L} C_{ab21}^{T,L*} + C_{ab12}^{S,L} C_{ab12}^{T,L*} \right) \right) \Big] , \tag{28}
\end{aligned}$$

with the theta function in terms of q^2 and k^2 defined as

$$\begin{aligned}
\Theta_{\text{L. inv.}}(q^2, k^2) \Big|_{m_a=m_b=0} = & \theta(q^2) \theta((m_K - m_\pi)^2 - q^2) \\
& \times \theta \left(k^2 - \frac{1}{2} (m_K^2 + m_\pi^2 - q^2 - \lambda_{K\pi q^2}^{1/2}) \right) \\
& \times \theta \left(\frac{1}{2} (m_K^2 + m_\pi^2 - q^2 + \lambda_{K\pi q^2}^{1/2}) - k^2 \right) . \tag{29}
\end{aligned}$$

For massless Dirac neutrinos we similarly find

$$\begin{aligned}
\frac{d^2\Gamma_{ab}}{dq^2 dk^2} &= \frac{1}{256\pi^3 m_K^3} \Theta_{\text{L. inv.}}(q^2, k^2) \Big|_{m_a=m_b=0} \\
&\times \left(- (f^V(q^2))^2 (k^4 - k^2(m_K^2 + m_\pi^2 - q^2) + m_K^2 m_\pi^2) \right. \\
&\quad \times \left(\left| C_{ab12}^{V,LL,\text{SM}} + C_{ab12}^{V,LL} + C_{ab12}^{V,LR} \right|^2 + \left| C_{ab12}^{V,RL} + C_{ab12}^{V,RR} \right|^2 \right) \\
&+ \frac{q^2}{4} \left((F^S(q^2))^2 \left(\left| C_{ab12}^{S,LL} + C_{ab12}^{S,LR} \right|^2 + \left| C_{ba21}^{S,LR} + C_{ba21}^{S,LL} \right|^2 \right) \right. \\
&\quad \left. + (F^T(q^2))^2 (-2k^2 + m_K^2 + m_\pi^2 - q^2)^2 \left(\left| C_{ab12}^{T,LL} \right|^2 + \left| C_{ba21}^{T,LL} \right|^2 \right) \right) \\
&- \frac{q^2}{2} (-2k^2 + m_K^2 + m_\pi^2 - q^2) \left(\right. \\
&\quad + F^S(q^2) F^T(q^2) \text{Im} \left(C_{ab12}^{T,LL} \left(C_{ba21}^{S,LL} + C_{ba21}^{S,LR} \right) \right) \\
&\quad + F^S(q^2) (F^T(q^2))^* \text{Im} \left(C_{ba21}^{T,LL*} \left(C_{ba21}^{S,LL} + C_{ba21}^{S,LR} \right) \right) \\
&\quad + (F^S(q^2))^* F^T(q^2) \text{Im} \left(C_{ab12}^{T,LL} \left(C_{ab12}^{S,LL} + C_{ab12}^{S,LR} \right)^* \right) \\
&\quad \left. + (F^S(q^2))^* (F^T(q^2))^* \text{Im} \left(C_{ba21}^{T,LL*} \left(C_{ab12}^{S,LL} + C_{ab12}^{S,LR} \right)^* \right) \right) \Bigg). \tag{30}
\end{aligned}$$

Note, that for massless neutrinos the interference term between the scalar and tensor operators vanishes for both Majorana, and Dirac neutrinos, after integration over the full k^2 phase space, which is why such terms do not appear in Eqs. (21) and (23).

References

- [1] E. Cortina Gil, A. Kleimenova, E. Minucci, S. Padolski, P. Petrov, A. Shaikhiev et al., *An investigation of the very rare $K^+ \rightarrow \pi^+ \nu \bar{\nu}$ decay*, *Journal of High Energy Physics* **2020** (Nov., 2020) .
- [2] NA62 collaboration, E. Cortina Gil et al., *Measurement of the very rare $K^+ \rightarrow \pi^+ \nu \bar{\nu}$ decay*, *JHEP* **06** (2021) 093, [2103 . 15389].
- [3] KOTO collaboration, J. K. Ahn et al., *Search for the $K_L \rightarrow \pi^0 \nu \bar{\nu}$ and $K_L \rightarrow \pi^0 X^0$ decays at the J-PARC KOTO experiment*, *Phys. Rev. Lett.* **122** (2019) 021802, [1810 . 09655].
- [4] KOTO collaboration, J. K. Ahn et al., *Study of the $K_L \rightarrow \pi^0 \nu \bar{\nu}$ Decay at the J-PARC KOTO Experiment*, *Phys. Rev. Lett.* **126** (2021) 121801, [2012 . 07571].
- [5] E. Goudzovski et al., *New physics searches at kaon and hyperon factories*, *Rept. Prog. Phys.* **86** (2023) 016201, [2201 . 07805].
- [6] G. Anzivino et al., *Workshop summary – Kaons@CERN 2023*, in *Kaons@CERN 2023*, 11, 2023, 2311 . 02923.
- [7] S. L. Glashow, J. Iliopoulos and L. Maiani, *Weak Interactions with Lepton-Hadron Symmetry*, *Phys. Rev. D* **2** (1970) 1285–1292.
- [8] G. Buchalla and A. J. Buras, *The rare decays $K \rightarrow \pi \nu \bar{\nu}$, $B \rightarrow X \nu \bar{\nu}$ and $B \rightarrow l^+ l^-$: An Update*, *Nucl. Phys. B* **548** (1999) 309–327, [hep-ph/9901288].
- [9] M. Misiak and J. Urban, *QCD corrections to FCNC decays mediated by Z penguins and W boxes*, *Phys. Lett. B* **451** (1999) 161–169, [hep-ph/9901278].
- [10] A. J. Buras, M. Gorbahn, U. Haisch and U. Nierste, *Charm quark contribution to $K^+ \rightarrow \pi^+ \nu \bar{\nu}$ at next-to-next-to-leading order*, *JHEP* **11** (2006) 002, [hep-ph/0603079].
- [11] F. Mescia and C. Smith, *Improved estimates of rare K decay matrix-elements from K_{l3} decays*, *Phys. Rev. D* **76** (2007) 034017, [0705 . 2025].
- [12] J. Brod and M. Gorbahn, *Electroweak Corrections to the Charm Quark Contribution to $K^+ \rightarrow \pi^+ \nu \bar{\nu}$* , *Phys. Rev. D* **78** (2008) 034006, [0805 . 4119].
- [13] J. Brod, M. Gorbahn and E. Stamou, *Two-Loop Electroweak Corrections for the $K \rightarrow \pi \nu \bar{\nu}$ Decays*, *Phys. Rev. D* **83** (2011) 034030, [1009 . 0947].
- [14] G. Isidori, F. Mescia and C. Smith, *Light-quark loops in $K \rightarrow \pi \nu \bar{\nu}$* , *Nucl. Phys. B* **718** (2005) 319–338, [hep-ph/0503107].
- [15] Z. Bai, N. H. Christ, X. Feng, A. Lawson, A. Portelli and C. T. Sachrajda, *$K^+ \rightarrow \pi^+ \nu \bar{\nu}$ decay amplitude from lattice QCD*, *Phys. Rev. D* **98** (2018) 074509, [1806 . 11520].
- [16] RBC, UKQCD collaboration, N. H. Christ, X. Feng, A. Portelli and C. T. Sachrajda, *Lattice QCD study of the rare kaon decay $K^+ \rightarrow \pi^+ \nu \bar{\nu}$ at a near-physical pion mass*, *Phys. Rev. D* **100** (2019) 114506, [1910 . 10644].
- [17] J. Brod, M. Gorbahn and E. Stamou, *Updated standard model prediction for $k \rightarrow \pi \nu \bar{\nu}$ and ϵ_k* , 2021.

- [18] PARTICLE DATA GROUP collaboration, R. L. Workman, *Review of Particle Physics*, *PTEP* **2022** (2022) 083C01.
- [19] HIKE collaboration, M. U. Ashraf et al., *High Intensity Kaon Experiments (HIKE) at the CERN SPS Proposal for Phases 1 and 2*, *2311.08231*.
- [20] KOTO collaboration, H. Nanjo, *KOTO II at J-PARC : toward measurement of the branching ratio of $K_L \rightarrow \pi^0 \nu \bar{\nu}$* , *J. Phys. Conf. Ser.* **2446** (2023) 012037.
- [21] D. Aristizabal Sierra, V. De Romeri and N. Rojas, *COHERENT analysis of neutrino generalized interactions*, *Phys. Rev. D* **98** (2018) 075018, [*1806.07424*].
- [22] W. Altmannshofer, M. Tamaro and J. Zupan, *Non-standard neutrino interactions and low energy experiments*, *JHEP* **09** (2019) 083, [*1812.02778*].
- [23] A. Falkowski, M. González-Alonso and Z. Tabrizi, *Reactor neutrino oscillations as constraints on Effective Field Theory*, *JHEP* **05** (2019) 173, [*1901.04553*].
- [24] I. Bischer and W. Rodejohann, *General neutrino interactions from an effective field theory perspective*, *Nucl. Phys. B* **947** (2019) 114746, [*1905.08699*].
- [25] T. Han, J. Liao, H. Liu and D. Marfatia, *Scalar and tensor neutrino interactions*, *JHEP* **07** (2020) 207, [*2004.13869*].
- [26] A. Abada, D. Bečirević, O. Sumensari, C. Weiland and R. Zukanovich Funchal, *Sterile neutrinos facing kaon physics experiments*, *Phys. Rev. D* **95** (2017) 075023, [*1612.04737*].
- [27] E. E. Jenkins, A. V. Manohar and P. Stoffer, *Low-Energy Effective Field Theory below the Electroweak Scale: Operators and Matching*, *JHEP* **03** (2018) 016, [*1709.04486*].
- [28] F. F. Deppisch, K. Fridell and J. Harz, *Constraining lepton number violating interactions in rare kaon decays*, *JHEP* **12** (2020) 186, [*2009.04494*].
- [29] G. Buchalla, A. J. Buras and M. E. Lautenbacher, *Weak decays beyond leading logarithms*, *Rev. Mod. Phys.* **68** (1996) 1125–1144, [*hep-ph/9512380*].
- [30] H. K. Dreiner, H. E. Haber and S. P. Martin, *Two-component spinor techniques and Feynman rules for quantum field theory and supersymmetry*, *Phys. Rept.* **494** (2010) 1–196, [*0812.1594*].
- [31] A. Denner, H. Eck, O. Hahn and J. Kublbeck, *Compact Feynman rules for Majorana fermions*, *Phys. Lett. B* **291** (1992) 278–280.
- [32] R.-X. Shi et al., *Revisiting the new-physics interpretation of the $b \rightarrow c \tau \nu$ data*, *Journal of High Energy Physics* **2019** (12, 2019) .
- [33] I. Baum et al., *Matrix elements of the electromagnetic operator between kaon and pion states*, *Physical Review D* **84** (10, 2011) .
- [34] F. Brizioli, *Measurement of $Br(K^+ \rightarrow \pi^+ \nu \bar{\nu})$ with the NA62 experiment at CERN*, Ph.D. thesis, Perugia U., 2021.
- [35] E. Cortina Gil, E. Minucci, S. Padolski, P. Petrov, B. Velghe, G. Georgiev et al., *First search for $k^+ \rightarrow \pi^+ \nu \bar{\nu}$ using the decay-in-flight technique*, *Physics Letters B* **791** (Apr., 2019) 156–166.

- [36] W. A. Rolke, A. M. Lopez and J. Conrad, *Limits and confidence intervals in the presence of nuisance parameters*, *Nucl. Instrum. Meth. A* **551** (2005) 493–503, [[physics/0403059](#)].
- [37] K. Cranmer, *Practical Statistics for the LHC*, in *2011 European School of High-Energy Physics*, pp. 267–308, 2014, [1503.07622](#), DOI.
- [38] HIKE collaboration, E. Cortina Gil et al., *HIKE, High Intensity Kaon Experiments at the CERN SPS: Letter of Intent*, [2211.16586](#).
- [39] M. Gorbahn, U. Moldanazarova, K. H. Sieja, E. Stamou and M. Tabet, *in preparation*, .
- [40] https://gitlab.com/manstam/kpinunu_distributions_in_left, 2023.